



Rickards, A. M. J., Miles, R. E. H., Davies, J. F., Marshall, F. H., & Reid, J. P. (2013). Measurements of the Sensitivity of Aerosol Hygroscopicity and the kappa Parameter to the O/C Ratio. *Journal of Physical Chemistry A*, 117(51), 14120-14131. 10.1021/jp407991n

Link to published version (if available):
[10.1021/jp407991n](https://doi.org/10.1021/jp407991n)

[Link to publication record in Explore Bristol Research](#)
PDF-document

University of Bristol - Explore Bristol Research

General rights

This document is made available in accordance with publisher policies. Please cite only the published version using the reference above. Full terms of use are available:
<http://www.bristol.ac.uk/pure/about/ebr-terms.html>

Take down policy

Explore Bristol Research is a digital archive and the intention is that deposited content should not be removed. However, if you believe that this version of the work breaches copyright law please contact open-access@bristol.ac.uk and include the following information in your message:

- Your contact details
- Bibliographic details for the item, including a URL
- An outline of the nature of the complaint

On receipt of your message the Open Access Team will immediately investigate your claim, make an initial judgement of the validity of the claim and, where appropriate, withdraw the item in question from public view.

1 **Measurements of the Sensitivity of Aerosol Hygroscopicity**
2 **and the Kappa Parameter to the O/C Ratio**

3
4 Andrew M. J. Rickards, Rachael E. H. Miles, James F. Davies, Frances H. Marshall and Jonathan P. Reid*

5 *School of Chemistry, University of Bristol, Bristol, BS8 ITS, UK*

6
7 **ABSTRACT**

8 We report measurements of the subsaturated hygroscopic growth of aerosol particles composed of single
9 organic components of varying oxygen-to-carbon ratio up to relative humidities approaching saturation using
10 the techniques of aerosol optical tweezers and an electrodynamic balance. The variation in the
11 hygroscopicity parameter κ between compounds of even the same O/C ratio is found to be significant with,
12 for example, a range in κ values from 0.12 to 0.38 for compounds with an O/C of 1. The measurements are
13 compared with a review of all of the available literature data for which both the κ value and O/C ratio are
14 reported and a new parameterisation determined. Critical supersaturations predicted using this
15 parameterisation yield values that have associated uncertainties that are comparable to typical uncertainties
16 in experimental measurements of critical supersaturations. However, the systematic variability between κ
17 parameterisations determined from different studies remains large, consistent with the O/C ratio providing
18 only an approximate guide to aerosol hygroscopicity and reflecting significant variations for aerosols of
19 different chemical functionality, composition and oxidation history.

20
21 Keywords: Aerosol, single particle, hygroscopicity, organic aerosol, thermodynamics

22
23
24
25
26
27
28 * Corresponding author: j.p.reid@bristol.ac.uk, tel: +44 117 331 7388

29 I. INTRODUCTION

30 Aerosols play an important role in influencing radiative forcing through both the direct effect, where the
31 aerosol particles directly scatter and absorb radiation, and the indirect effect, where the aerosol particles act
32 as cloud condensation nuclei (CCN) and influence cloud droplet number concentrations, size distributions
33 and lifetime.¹⁻³ Understanding the response of aerosol particle size and composition to changes in relative
34 humidity (RH) is crucial to quantifying their chemical, physical and optical properties and to reducing the
35 large uncertainty in the magnitude of the aerosol indirect effect.⁴ An aerosol responds to an increase in
36 relative humidity through the increased partitioning of water into the condensed phase, maintaining
37 equilibrium between the gas and liquid phases. At the microphysical level, an individual aerosol particle
38 grows to a wet diameter $D(RH)$ that is usually referenced to the diameter of the particle under dry conditions,
39 D_0 , a ratio referred to as the growth factor, $GF (= D(RH)/D_0)$. The dry size reflects the amount of involatile
40 solute associated with the aerosol particle.

41

42 Characterising the hygroscopic growth of ambient aerosol has become a routine analytical measurement for
43 accumulation mode particles through the use, for example, of an hygroscopic tandem differential mobility
44 analyser (HTDMA).⁵⁻⁷ The aerosol sample must be dried before passing it through a first DMA to select a
45 narrow range of particle sizes. The dry aerosol is then humidified under a high RH and passed into a second
46 DMA, which is used to measure the equilibrium size at the elevated RH. In the laboratory, measurements of
47 equilibrium hygroscopic growth on single or multiple component aerosol are performed using ensemble (eg.
48 HTDMA) and single particle techniques (eg. electrodynamic balance and optical tweezers),⁸⁻¹¹ providing
49 controlled studies that can be used to robustly test equilibrium state models and interpret ambient field
50 measurements.

51

52 The hygroscopic growth of individual inorganic and organic component aerosol can be rigorously treated
53 with well-established models¹²⁻¹⁷ and with approximate treatments derived to capture the phase
54 behaviour.^{18,19} One such simplified framework is κ -Köhler theory,¹⁸ a quantitative model describing the
55 degree of hygroscopic growth for an aerosol component by a single hygroscopicity parameter, κ . This
56 parameter can be derived from hygroscopic growth measurements made under subsaturated conditions and
57 can be inferred from the critical supersaturation required to achieve activation of cloud condensation nuclei

58 (CCN) under supersaturated conditions. For organic species, κ is usually between 0 (non-hygroscopic) and
59 0.5 (very hygroscopic).¹⁸ Organic components form a substantial proportion of atmospheric aerosol, between
60 20 and 90 % of the submicron mass depending on region,^{20,21} and consists of an enormous variety of
61 different species with a wide range of functional groups for which the hygroscopic properties of only a
62 handful are well characterised.^{22,23} Attributing contributions to the hygroscopic growth of ambient aerosol
63 from individual compounds is an intractable approach and the application of a more simplistic model, such
64 as κ -Köhler theory, is unavoidable. A necessary caveat is that more complex models should be applied
65 whenever possible to assess and quantify the level of uncertainty that is acceptable. For example, the change
66 in partitioning of semi-volatile organic components with RH,²⁴ the occurrence of liquid-liquid phase
67 separation,²⁵ and the surface tension depression of droplets by surfactants²⁶ are all examples of
68 thermodynamic properties that still require further detailed investigation.

69

70 For subsaturated growth, κ is defined by Petters & Kreidenweis¹⁸ by the parameterisation:

$$71 \quad GF = \left(1 + \kappa \frac{a_w}{1 - a_w} \right)^{\frac{1}{3}} \quad (1)$$

72 where a_w is the water activity in the gas phase. This expression is stated in the large particle limit, where the
73 effect of surface curvature can be neglected, and the water activity can be assumed to be equal to the RH. A
74 constant osmotic coefficient must be assumed, an assumption that breaks down as the RH decreases and non-
75 ideality in solute/solvent interactions becomes important. Not only can this framework for quantifying
76 hygroscopicity be used for binary solution aerosol containing a single solute and water, but standard mixing
77 rules such as the Zdanovskii, Stokes, and Robinson (ZSR) assumption can be used to predict the
78 hygroscopicity of mixed component aerosol.²⁷ To estimate κ from hygroscopic growth measurements it is
79 common practice to make measurements at high RH (0.9 or larger). Petters & Kriedenweis²⁸ reported that κ
80 values estimated from hygroscopic growth and critical supersaturation measurements agreed to within 30 %,
81 suggesting that the change in κ measured at a water activity, a_w , of 0.9 to the value at the water activity
82 corresponding to activation is small. Although a large number of more recent studies have found consistency
83 (within 10 - 30 %) for the values of κ estimated from subsaturated and supersaturated measurements,^{9,18,29-35}
84 larger discrepancies have been found in a significant number of studies.³⁶⁻⁴² The discrepancies have been

85 attributed to the non-ideal behaviour for supersaturated solutions of solutes,^{43,44} the possibility of kinetic
86 limitations on particle drying and the estimation of the dry particle size,^{45,46} incorrect assumptions about
87 surface tension effects,³⁶⁻⁴² and the slow dissolution of sparingly soluble compounds.^{44,47} However
88 determining the relative importance of these effects may prove difficult as recent research has also shown
89 instrument dependent discrepancies in κ values determined for secondary organic aerosol (SOA).^{46,48}

90
91 Quantifying the accuracy of any hygroscopicity model for predicting the critical supersaturation for
92 activation of CCN is crucially important for understanding laboratory measurements and the formation of
93 cloud droplets from ambient aerosol.⁴⁹ At activation, the water activity in an aerosol particle is typically
94 larger than 0.99 and approaches a value of 1. Indeed, under such limiting conditions it is important that the
95 functional forms chosen to reproduce the hygroscopic response have the correct form to characterise the
96 limiting behaviour;⁵⁰ large uncertainties in the water activity at activation can result even from the
97 appropriateness of the parameterisation chosen to represent the relationship between water activity and solute
98 concentration (or mass fraction of solute).

99
100 Examples of the variability in the theoretical treatments of hygroscopicity for three typical single organic
101 component aerosol (malonic acid, levoglucosan and adipic acid) are shown in Figure 1, using four well-
102 established models. The Extended Aerosol Inorganics Model (E-AIM) was implemented by Clegg et al. to
103 treat the solution thermodynamics of the $\text{H}^+\text{-NH}_4^+\text{-Na}^+\text{-SO}_4^{2-}\text{-NO}_3^-\text{-Cl}^-\text{-H}_2\text{O}$ system.^{12,14} It was later extended
104 to include organic components using the widely used UNiversal quasichemical Functional-group Activity
105 Coefficient (UNIFAC) model.⁵¹ In some cases, the parameters for certain functional groups have been
106 modified according to measurements made on single organic aerosol particles using an electrodynamic
107 balance by Peng et al.¹³ The Aerosol Diameter Dependent Equilibrium Model (ADDEM) was developed by
108 Topping et al. to describe the thermodynamic behaviour of mixed inorganic salts and is coupled with a
109 diameter dependent Kelvin term to account for surface curvature.¹⁵ The thermodynamic relationships
110 describing water partitioning with varying RH assume the same parametric dependence as E-AIM for
111 inorganic components and UNIFAC for organic components. The Aerosol Inorganic-Organic Mixtures
112 Functional groups Activity Coefficients model (AIOMFAC) is a further group contribution model designed

113 to determine activity coefficients of chemical species within aerosols containing atmospherically relevant
114 inorganic-organic mixtures and accounts for the interactions of ions and neutral compounds.^{16,17}

115

116 Although there is considerable variation in the subsaturated growth curves calculated from the models for the
117 three compounds shown in Figure 1, the growth curves are comparable in the dilute solute limit, particularly
118 for the models that are considered to be more reliable (i.e. excluding UNIFAC without the Peng correction).
119 Using equation (1) we can estimate the apparent variation in the value of κ that would be retrieved if these
120 models were used to infer the hygroscopicity parameter at RHs other than at saturation on approach to
121 infinite dilution of the solute; the apparent κ depends strongly on the water activity even at values
122 approaching saturation and varies considerably from system to system. An increase in κ at high RH, as seen
123 in Figure 1, has previously been attributed to the effects of surface activity and non-idealities in the
124 droplets.^{26,52} However, in the current simulations the qualitative shape of the dependence of κ on RH reflects
125 deviations from non-ideal behaviour with no accounting for surface tension depression. Even subtle changes
126 in the slope of the growth curve near 100 % RH can significantly alter the value of κ that would be
127 calculated from fitting to equation (1).

128

129 In the atmosphere, organic compounds can undergo both functionalisation reactions, notably oxidation to
130 form lower volatility compounds with an increased stoichiometric ratio of oxygen to carbon atoms in a
131 compound (O/C), and fragmentation reactions that lead to higher volatility compounds. The partitioning of
132 semi-volatile and lower volatility organic compounds to the condensed phase leads to the production of
133 SOA. As might be intuitively expected, the hygroscopicity of ambient and chamber SOA, as quantified by
134 the measured value of κ , has been found to correlate with the O/C ratio.^{7,20,53} The O/C ratio is conveniently
135 derived from the relative abundance of the ion signal m/z 44 in Aerodyne aerosol mass spectrometry (AMS)
136 measurements of aerosol composition.²⁰ The m/z 44 signal can be largely attributed to the CO_2^+ ion
137 fragment, and the fraction of the total organic signal due to the m/z 44 ion fragment, f_{44} , has been shown to
138 vary linearly with O/C by the Aiken et al. parameterisation.^{7,54}

139

140 Our aim here is to examine the relationship between O/C and κ for a range of organic functional groups
141 through a series of new laboratory measurements for organic components of selected O/C ratios. We also
142 provide a comprehensive review of the literature, summarising all previous measurements of κ when the
143 composition of the aerosol, represented by its O/C ratio, has also been reported, spanning the range from
144 around 0 to 2. The literature review encompasses a wide variety of systems spanning field measurements,
145 chamber SOA studies, and single particle laboratory studies, providing data from both natural and
146 synthesised multi-component particles, as well as single component aerosol. Finally, we look at the
147 variability in κ that can be expected for compounds of the same O/C ratio and the implications of this
148 variability for predictions of the critical supersaturation.

149

150 **II. SINGLE PARTICLE MEASUREMENTS OF SUBSATURATED HYGROSCOPIC GROWTH**

151 We have used two experimental techniques to measure the hygroscopic growth of binary and multi-
152 component aqueous solution droplets containing a range of organic compounds with varying O/C ratio.
153 Using the aerosol optical tweezers technique, we report the equilibrium response in particle size to changes
154 in RH up to a maximum water activity of 0.85. In the second technique, we use an electrodynamic balance to
155 retrieve the hygroscopic growth curve from fast measurements of evaporation kinetics from dilute aqueous
156 solution droplets. This approach allows measurements to be made at water activities as high as >0.99 .

157

158 *II.a Aerosol Optical Tweezers Measurements*

159 Initial measurements of hygroscopic growth using aerosol optical tweezers (AOT) focused on organic
160 aerosol components with O/C=1. A range of species with different functionalities and solubilities were
161 investigated to assess the comparability in their hygroscopic growth and values of κ . Single component
162 aerosol containing organic compounds with a broader range of O/C ratios were then explored, followed by
163 measurements of the hygroscopic properties of droplets containing mixtures of organic compounds. Table 1
164 summarises the compounds studied.

165

166 The aerosol optical tweezers experimental method has been described in detail in our previous
167 publications⁵⁵⁻⁵⁷ and will only be reviewed briefly here. A single beam gradient force optical trap (optical

168 tweezers) was formed within a custom built trapping chamber by passing continuous wave laser light at 532
169 nm through a microscope objective (Olympus oil immersion, $\times 100$). An aqueous solution of each organic
170 compound to be studied was nebulised in to the trapping chamber under a humidified nitrogen flow using an
171 ultrasonic nebuliser (Omron). A single particle was captured from the aerosol plume and trapped at the focal
172 point of the laser beam. Inelastic Raman scattering, Stoke's shifted from the laser wavelength, from chemical
173 species within the droplet was collected by the microscope objective and coupled into a spectrograph
174 (Princeton Instruments). Raman spectra from the trapped droplet were collected every second. An image of
175 the droplet was also recorded using conventional brightfield microscopy. By altering the ratio of wet to dry
176 nitrogen flows, the RH of the environment inside the trapping chamber was varied stepwise between 55 %
177 and 85 %. The trapped droplet was allowed to fully equilibrate after each step change in relative humidity
178 and its hygroscopic response recorded. Accurate measurement of the RH was made using two probes, one
179 before (Vaisala; ± 2 % RH) and one after (Honeywell; ± 2 % RH) the trapping chamber.

180

181 The spectroscopic signature from the tweezed aerosol consists of broad spontaneous Stokes bands arising
182 from the Raman excitation of vibrational modes of the molecular constituents of the droplet. Superimposed
183 on this spontaneous scattering background, the Raman intensity is amplified at wavelengths commensurate
184 with whispering gallery modes, providing a unique fingerprint of resonant wavelengths that can be compared
185 with Mie scattering calculations to retrieve both the droplet size and refractive index, both with uncertainties
186 of ± 0.05 %.^{58,59} A typical variation in droplet size and refractive index with changing RH profile is shown in
187 Figure 2 for hygroscopicity measurements on an aqueous sucrose droplet. The figure shows a clear decrease
188 in size and increase in refractive index as the RH is decreased and water evaporates from the droplet.

189

190 To convert the droplet radial data into a *GF* it is necessary to know the solute dry diameter, D_0 . This was
191 determined from the volume fraction of organic in the droplet, $V_{f,org}$, estimated from the retrieved refractive
192 index and the total droplet volume, as given by the droplet diameter. Assuming the refractive index of the
193 aqueous organic droplet at a particular RH, RI_{drop} , is the linear sum of the refractive indices of the pure
194 organic component, RI_{org} , and water, RI_w , weighted by their volume fractions present within the droplet, $V_{f,org}$
195 can be calculated using:

196 $RI_{drop} = RI_{org}V_{f,org} + RI_wV_{f,w}$ (2)

197 where $V_{f,w}$ is the volume fraction of water in the droplet ($1-V_{f,org}$) and RI_{drop} is determined from the Raman
 198 spectra at each RH. The pure refractive indices for the organic compounds of interest were obtained by
 199 measuring the refractive index of a series of aqueous solutions of the organic with increasing mass fraction
 200 of solute (mfs) using a refractometer (MISCO Palm Abbe). Solutions were made up to the bulk solubility
 201 limit for each compound. From a quadratic fit, the refractive index was estimated at an extrapolated mfs = 1
 202 to determine RI_{org} (Figure 3). Where possible, values determined by this approach were compared with
 203 literature values. An estimate of the typical level of uncertainty associated with such extrapolations is
 204 indicated in Figure 3.

205

206 For solutions containing more than one organic component, the contribution in volume weighted refractive
 207 index of each solute, i , was considered separately:

208 $RI_{org} = \frac{1}{V_{org}} \sum_i RI_i V_i$ (3)

209 $V_{f,org} = \frac{RI_{drop} - RI_w}{\frac{1}{V_{org}} \sum_i RI_i V_i - RI_w}$ (4)

210 For both binary and multicomponent aerosol, a value of D_0 was determined from the particle radius and
 211 refractive index pairing retrieved from the Raman spectra at every RH step, with the mean and standard
 212 deviation of these values then taken to give an average value for D_0 , along with an associated error, σ . The
 213 mean value of D_0 was used to convert measured wet size to a GF , with this then used in equation (1) to
 214 determine a value of κ for the organic compound at each a_w for which measurements were taken. Upper and
 215 lower bounds were placed on the retrieved κ values by performing the same calculation using dry particle
 216 diameters of $D_0 \pm \sigma$ to calculate the GFs.

217

218 *II.b Electrodynamic Balance Measurements*

219 The equilibrium hygroscopic properties of aerosol play a key role in the mass transfer dynamics of water
 220 between the droplet and gas phase.⁶⁰ Indeed, we have shown that measurements of the evaporation rate of
 221 water from aerosol droplets of known composition may be used to determine hygroscopic growth of aerosol

222 at water activities approaching saturation.⁶¹ We use the same approach here and only briefly review the
223 technique. Using an electrodynamic balance held at a fixed RH and temperature, measurements of water
224 evaporation from aerosol droplets of two compositions were rapidly studied in sequence, introducing the
225 droplets from two droplet-on-demand micro-dispensers (Figure 4a). Following the evaporation of a pure
226 water droplet, which was used as a probe/control for determining the gas phase conditions, a droplet
227 containing a sample solute was introduced and its approach to equilibrium monitored. The time-
228 dependencies in droplet radii were determined with 10 ms time-resolution from the angular fringe spacing in
229 the elastic scattering pattern using a geometrical optic approximation.⁶² Changes in refractive index were
230 accounted for in a post-analysis step,⁶³ and the average evaporation trends for multiple droplets of both probe
231 and sample solutions were found.

232

233 The evaporation rate of pure water from the control droplet was used to estimate the RH in the gas phase,
234 using the equations of Kulmala et al. to simulate the evaporation kinetics, with an accuracy in the gas phase
235 water activity of around ± 0.001 at 0.95 and ± 0.003 at 0.90.^{64,65} The evaporation of the sample solution
236 droplets took place under identical conditions given the timescales of the measurements. A simple volume
237 additive approach to treating the solution density was employed to determine the mass flux at every time
238 resolved radius and, from estimates of the initial size and mass concentration, a dry size was determined and
239 a growth factor at every radius deduced (Figure 4b (inset)). Under the assumption that gas phase diffusion
240 was the limiting process in evaporation (a valid assumption given the insensitivities to surface processes and
241 the non-viscous nature of the particles),⁶⁰ the equations of Kulmala et al. were used to calculate, using the
242 RH and mass flux, the water activity of the droplet at every size. The results of this procedure were averaged
243 and are shown against growth factor in Figure 4b. This procedure has been demonstrated in our previous
244 work⁶¹ and is used here as a way of determining hygroscopicity at water activities approaching unity. The
245 sensitivity of the droplet evaporation measurements to different values of κ is illustrated in Figure 5(a),
246 clearly indicating the differences in hygroscopicity which can be resolved by the comparative kinetic
247 technique. For comparison, the evaporation profiles for two compounds with different values of κ are shown
248 in Figure 5(b). These are intended only as examples and it should be noted that the two measurements are
249 into marginally different RHs and the droplets follow different variations in density with composition.

250

251 **IV. RESULTS AND DISCUSSION**

252 In Figure 6 we report the experimentally determined κ values retrieved at different values of water activity
253 for selected compounds studied with varying O/C. Values estimated from both the AOT (with a_w between
254 0.55 - 0.8) and EDB (with $a_w > 0.9$) techniques are shown. As apparent from the data, the techniques are in
255 good agreement and provide consistent values of κ as the same a_w is approached, indicated by linear fits to
256 the data used to guide the eye. Although no increase in κ at very high water activity can be discerned within
257 experimental error as infinite dilution is approached, an increase in the apparent κ is observed as the RH/a_w
258 decreases. The retrieval of an apparent dependence of κ on a_w provides a clear demonstration of the
259 limitations of the κ -Köhler model at relative humidities below the dilute limit when solution non-ideality
260 becomes significant and the assumptions inherent to the theory no longer apply. The sensitivity of the κ
261 value to the a_w of the measurement varies from compound to compound, as demonstrated by the five
262 representative compounds shown in Figure 6. The κ values determined from the EDB measurements show
263 excellent self-consistency over the limited range of high a_w measurements.

264

265 A single value of κ was determined from the AOT measurements by calculating the GF at the highest
266 measured RH and converting it using the κ -Köhler equation. An associated uncertainty was derived from the
267 uncertainty in the pure organic refractive index (from the extrapolation in Figure 3) and the standard
268 deviation of the dry size. Single values of κ were determined from the EDB measurements by averaging over
269 the values determined at each a_w , with the uncertainty then given by the standard deviation in these values.
270 We summarise the values estimated from the AOT and EDB measurements in Figure 7 and Table 1: a clear
271 general trend of increasing hygroscopicity with increasing O/C is observed, consistent with previous
272 observations.^{7,53,66-69}

273

274 We have undertaken an extensive review of κ values published in the literature (also shown in Figure 7)
275 encompassing a wide range of measurements that have included ensemble field measurements, chamber
276 SOA studies, and single particle measurements, which have yielded data for multicomponent atmospheric
277 aerosol, analogous laboratory-generated systems, and individual pure component particles, respectively (see

278 Supplementary Information, Table 1). The measurement techniques used to determine κ can be divided
279 according to those operating in the subsaturated regime ($RH < 100\%$) and in the supersaturated regime (RH
280 $> 100\%$). In the subsaturated regime, the majority of literature studies used an HTDMA to determine the
281 hygroscopic properties of ensemble aerosol.^{5–7,18–20,69–75} Other subsaturated techniques that have been used
282 included aerosol optical tweezers,⁸ electrodynamic balances,^{9–11} cavity ring down spectroscopy,⁶⁸ a
283 differential aerosol sizing and hygroscopicity spectrometer probe (DASH-SP),^{76,77} the Leipzig Aerosol Cloud
284 Interaction Simulator (LACIS),⁷⁸ and a continuous-flow thermal gradient column (CFTGC).⁵² Measurements
285 in the supersaturated regime were mostly performed using a cloud condensation nuclei counter (CCNC),
286 inferring the hygroscopicity parameter from critical supersaturations.^{18,19,53,66,67,75,79–89} In this technique, a
287 narrow size fraction of the aerosol sample to be studied is selected using, for example, a DMA or a virtual
288 impactor and exposed to a chosen supersaturation. The ratio of the number of aerosol particles that activate
289 to the total number of particles exposed to the supersaturation is then calculated. By scanning through
290 different supersaturations, the critical supersaturation is determined as the value at which 50% of the aerosol
291 particles activate, which can then be used to estimate κ . In the vast majority of the literature studies, the O/C
292 for the aerosol was determined from aerosol mass spectrometer (AMS) f_{44} values according to the Aiken et
293 al. parameterisation.^{5–7,20,53,66–69,71–73,75–85,87–89} In other cases the chemical composition of the aerosol was well
294 defined and thus the O/C was calculated from the molecular formula.^{8–11,18,19,52,70,74,86} The published studies
295 found in the literature reported κ values for aerosols with O/C ranging from around 0 to 2.

296

297 The data identified in the literature review show a general positive correlation between κ and O/C, although
298 it is not possible to represent the relationship between κ and O/C with a simple linear parameterisation
299 (Figure 7). In order to identify whether specific measurement regimes or types of aerosol sample could lead
300 to systematic variations in the value of κ , the literature data have been subdivided in three ways: a) according
301 to the saturation regime under which it was taken, b) the origin of the aerosol sample, and c) the method by
302 which the O/C was determined. These three divisions are shown as separate panels in Figure 8. It is clear that
303 regardless of the criterion used to divide the data, equivalent levels of variability in the value of κ for a given
304 O/C are observed from the literature data. Although the O/C ratio is a frequently used measure of aerosol
305 composition/age, Figures 7 and 8 suggest that it is a poor indicator of hygroscopicity. This conclusion is

306 supported by the AOT and EDB measurements reported in this study, which mirror closely the degree of
307 scatter seen in the literature data, in particular the large variation in the value of κ seen in the measurements
308 for O/C = 1.

309

310 It is instructive to consider how the scatter in the values of κ at a given O/C would manifest itself as an
311 uncertainty in the predicted critical supersaturation for CCN activation if a linear parameterisation linking κ
312 and O/C was used to calculate this quantity. Figure 9a shows all of the data points presented in Figure 7
313 binned according to their O/C in intervals of 0.1, with the κ values taken as the average of all data points in
314 each O/C bin and the error bars showing the associated standard deviation. Any uncertainties in the κ values
315 reported in the original studies have been ignored and we consider only the minimum error that would be
316 introduced in to the critical supersaturation by use of a linear κ to O/C parameterisation. The grey shaded
317 region on Figure 9a indicates the uncertainty envelope for the linear best fit through both the literature and
318 new experimental κ data reported in this manuscript. The line of best fit is weighted by the standard
319 deviations at each O/C ratio. Also shown for comparison are two previously proposed sets of linear
320 parameterisations,^{7,53} which have been extrapolated to cover the same O/C range as the present study. The
321 previous parameterisations are significantly different in gradient from that determined from the average of
322 the available literature data, reflecting the much smaller data sets, limited range of organic species and
323 narrower O/C ranges on which they were based. A similar data binning and fitting procedure was also
324 performed for each of the data sub-sets (6 cases) identified in Figure 8 (Supplementary information Figure 1
325 and Table 2). Although the uncertainties in the correlations is much lower for aerosol of known composition
326 measured in the laboratory, as might be expected, the spread in the fitted correlations is such that no
327 definitive conclusions can be made from the comparison of sub-saturated growth and critical supersaturation
328 measurements.

329

330 In Figure 9b we report the sensitivity of the predicted critical supersaturations to the value of κ derived at
331 varying O/C from the different parameterisations shown in Figure 9a. The spread in the κ values from the
332 literature survey for aerosol of a particular O/C, ignoring experimental errors, leads to a spread in the
333 predicted critical supersaturations. Considering the data point at O/C = 0.56 in Figure 9b alone, the spread in

334 critical supersaturation arising from the error bar at this O/C ratio is -17% to $+34\%$ on a critical
335 supersaturation of 0.36% RH (where this is the value from a κ of 0.10 ± 0.05). This is equivalent to a range
336 of 0.30 to 0.48% RH in critical supersaturation for an activating particle of 100 nm diameter and is larger
337 than typical uncertainties in experimentally determined supersaturations, which are of the order $\pm 0.04\%$
338 RH.⁵³ However, the uncertainty in the new parameterisation provided here from fitting all of the literature
339 data over the whole O/C range yields uncertainties in the critical supersaturation that are comparable to the
340 errors associated with experimental measurements of supersaturations. Again at an O/C ratio of 0.56 , the
341 spread in critical supersaturations shown in Figure 9b is 0.33 to 0.43% for a particle of 100 nm diameter.
342 The envelope defining the parameterisation is:

$$343 \quad \kappa = (0.190 \pm 0.017) \times (O/C) - (0.0048 \pm 0.0139) \quad (5)$$

344 As a further sensitivity test, Figure 10 shows the uncertainty in critical supersaturation with O/C for particles
345 of three different diameters that would result from the uncertainty in the parameterisation of the dependence
346 of κ on O/C shown in Figure 9. CCN of different dry size become virtually indistinguishable in terms of their
347 critical supersaturation when they have a composition commensurate with low O/C.

348

349 From Figures 9 and 10, it can be concluded that a general parameterisation of the dependence of κ on O/C,
350 such as that shown by the grey envelope in Figure 9a, can provide an approximate yet appropriate indicator
351 of the critical supersaturation and hygroscopic growth. Notably the variation in critical supersaturations
352 predicted by the different parameterisations for the O/C dependence of κ is considerably larger than
353 identified by the grey shaded envelope in Figure 9a. Given that the different parameterisations are based on
354 measurements performed on aerosols of different organic precursor type and oxidation mechanism, the
355 disparity between them does suggest that more accurate treatments of hygroscopic growth and CCN
356 activation must rely on different parameterisations for different chemical systems.

357

358 **V. SUMMARY**

359 We have reported new measurements of the hygroscopicity parameter κ for chemical compounds with a
360 range of O/C values and differing chemical functionalities. Measurements were made on single aerosol
361 particles using aerosol optical tweezers and an electrodynamic balance, with excellent agreement seen

362 between the two techniques. As the RH was decreased, deviation in the apparent κ from the constant value
363 seen at high a_w was observed, highlighting the need to make measurements of κ at high a_w in the dilute limit
364 where ideality can be assumed. The variation in the hygroscopicity parameter κ between compounds of even
365 the same O/C ratio is found to be significant with, for example, a range in κ values from 0.12 to 0.38 for
366 compounds with an O/C of 1.

367

368 A comprehensive review of all κ values published in the literature to date along with their associated O/C
369 ratios has been undertaken, encompassing field and laboratory studies, subsaturated and supersaturated
370 measurements, and multi-component and pure component aerosol. The literature data, combined with the
371 newly determined experimental values, showed a general positive correlation between κ and O/C, in
372 qualitative agreement with previously published results. We have presented a linear parameterisation of the
373 correlation between κ and O/C based on all of the published data for which both the κ value and O/C ratio
374 are known, showing a somewhat weaker dependence of κ on O/C than previous parameterisations. The
375 uncertainty in the predicted value of κ resulting from this parameterisation leads to an uncertainty in the
376 predicted critical supersaturation that is very similar to typical uncertainties associated with experimental
377 measurements of critical supersaturations. However, it should be stressed that significant variations are
378 observed between the κ vs O/C parameterisations derived from measurements with different aerosol types,
379 suggesting that the chemical complexity of a species hygroscopic response cannot be reliably captured by a
380 single parameter such as O/C.

381

382 **ACKNOWLEDGEMENTS**

383 We thank the Engineering and Physical Sciences Research Council for financial support through a
384 Leadership Fellowship awarded to JPR (grant reference EP/G007713/1). REHM acknowledges the National
385 Environmental Research Council for financial support (grant reference NE/1020075/1). Drs. Thomas Preston
386 and Jim Walker are acknowledge at the latter stages of this project for developing new software to determine
387 the size and refractive index of optically trapped droplets.

388

389 **Supporting Information Available**

390 Details of the literature review of hygroscopicity studies that report values of κ are given in the Supporting
391 Information, along with the additional fits described in Section IV. This information is available free of
392 charge via the Internet at <http://pubs.acs.org>

393 **REFERENCES**

- 394 (1) Twomey, S. The Influence of Pollution on the Shortwave Albedo of Clouds. *J. Atmos. Sci.* **1977**, *34*,
395 1149–1152.
- 396 (2) Albrecht, B. A. Aerosols, Cloud Microphysics, and Fractional Cloudiness. *Science* **1989**, *245*, 1227–
397 1230.
- 398 (3) Kanakidou, M.; Seinfeld, J. H.; Pandis, S. N.; Barnes, I.; Dentener, F. J.; Facchini, M. C.; Van
399 Dingenen, R.; Ervens, B.; Nenes, A.; Nielsen, C. J. et al. Organic Aerosol and Global Climate
400 Modelling: a Review. *Atmos. Chem. Phys.* **2005**, *5*, 1053–1123.
- 401 (4) Forster, P.; Ramaswamy, V.; Artaxo, P.; Berntsen, T.; Betts, R.; Fahey, D. W. 2007: Changes in
402 Atmospheric Constituents and in Radiative Forcing. In *Climate Change 2007: The Physical Science
403 Basis. Contribution of Working Group I to the Fourth Assessment Report of the Intergovernmental
404 Panel on Climate Change*; 2007; pp. 129–234.
- 405 (5) Alfarra, M. R.; Hamilton, J. F.; Wyche, K. P.; Good, N.; Ward, M. W.; Carr, T.; Barley, M. H.;
406 Monks, P. S.; Jenkin, M. E.; Lewis, A. C. et al. The Effect of Photochemical Ageing and Initial
407 Precursor Concentration on the Composition and Hygroscopic Properties of B-caryophyllene
408 Secondary Organic Aerosol. *Atmos. Chem. Phys.* **2012**, *12*, 6417–6436.
- 409 (6) Liu, Y.; Monod, A.; Tritscher, T.; Praplan, A. P.; DeCarlo, P. F.; Temime-Roussel, B.; Quivet, E.;
410 Marchand, N.; Dommen, J.; Baltensperger, U. Aqueous Phase Processing of Secondary Organic
411 Aerosol from Isoprene Photooxidation. *Atmos. Chem. Phys.* **2012**, *12*, 5879–5895.
- 412 (7) Duplissy, J.; DeCarlo, P. F.; Dommen, J.; Alfarra, M. R.; Metzger, A.; Barmapadimos, I.; Prevot, A. S.
413 H.; Weingartner, E.; Tritscher, T.; Gysel, M. et al. Relating Hygroscopicity and Composition of
414 Organic Aerosol Particulate Matter. *Atmos. Chem. Phys.* **2011**, *11*, 1155–1165.
- 415 (8) Dennis-Smith, B. J.; Hanford, K. L.; Kwamena, N.-O. A.; Miles, R. E. H.; Reid, J. P. Phase,
416 Morphology, and Hygroscopicity of Mixed Oleic Acid/sodium Chloride/water Aerosol Particles
417 Before and After Ozonolysis. *J. Phys. Chem. A* **2012**, *116*, 6159–68.
- 418 (9) Chan, M. N.; Kreidenweis, S. M.; Chan, C. K. Measurements of the Hygroscopic and Deliquescence
419 Properties of Organic Compounds of Different Solubilities in Water and Their Relationship with
420 Cloud Condensation Nuclei Activities. *Environ. Sci. Technol.* **2008**, *42*, 3602–8.
- 421 (10) Pope, F. D.; Tong, H.-J.; Dennis-Smith, B. J.; Griffiths, P. T.; Clegg, S. L.; Reid, J. P.; Cox, R. A.
422 Studies of Single Aerosol Particles Containing Malonic Acid, Glutaric Acid, and Their Mixtures with
423 Sodium Chloride. II. Liquid-State Vapor Pressures of the Acids. *J. Phys. Chem. A* **2010**, *114*, 10156–
424 10165.
- 425 (11) Pope, F. D.; Harper, L.; Dennis-Smith, B. J.; Griffiths, P. T.; Clegg, S. L.; Cox, R. A. Laboratory
426 and Modelling Study of the Hygroscopic Properties of Two Model Humic Acid Aerosol Particles. *J.
427 Aerosol Sci.* **2010**, *41*, 457–467.
- 428 (12) Clegg, S. L.; Brimblecombe, P.; Wexler, A. S. Thermodynamic Model of the System
429 $H^+-NH_4^+-Na^+-SO_4^{2-}-NO_3^- -Cl^- -H_2O$ at 298.15 K. *J. Phys. Chem. A* **1998**, *102*, 2155–2171.

- 430 (13) Peng, C.; Chan, M. N.; Chan, C. K. The Hygroscopic Properties of Dicarboxylic and Multifunctional
431 Acids: Measurements and UNIFAC Predictions. *Environ. Sci. Technol.* **2001**, *35*, 4495–501.
- 432 (14) Wexler, A. S.; Clegg, S. L. Atmospheric Aerosol Models for Systems Including the Ions H⁺, NH₄⁺,
433 Na⁺, SO₄²⁻, NO₃⁻, Cl⁻, Br⁻, and H₂O. *J. Geophys. Res.* **2002**, *107*.
- 434 (15) Topping, D. O.; McFiggans, G. B.; Coe, H. A Curved Multi-component Aerosol Hygroscopicity
435 Model Framework: Part 1 – Inorganic Compounds. *Atmos. Chem. Phys.* **2005**, *5*, 1205–1222.
- 436 (16) Zuend, A.; Marcolli, C.; Luo, B. P.; Peter, T. A Thermodynamic Model of Mixed Organic-inorganic
437 Aerosols to Predict Activity Coefficients. *Atmos. Chem. Phys.* **2008**, *8*, 4559–4593.
- 438 (17) Zuend, A.; Marcolli, C.; Booth, A. M.; Lienhard, D. M.; Soonsin, V.; Krieger, U. K.; Topping, D. O.;
439 McFiggans, G.; Peter, T.; Seinfeld, J. H. New and Extended Parameterization of the Thermodynamic
440 Model AIOMFAC: Calculation of Activity Coefficients for Organic-inorganic Mixtures Containing
441 Carboxyl, Hydroxyl, Carbonyl, Ether, Ester, Alkenyl, Alkyl, and Aromatic Functional Groups.
442 *Atmos. Chem. Phys.* **2011**, *11*, 9155–9206.
- 443 (18) Petters, M. D.; Kreidenweis, S. M. A Single Parameter Representation of Hygroscopic Growth and
444 Cloud Condensation Nucleus Activity. *Atmos. Chem. Phys.* **2007**, *7*, 1961–1971.
- 445 (19) Petters, M. D.; Kreidenweis, S. M.; Prenni, A. J.; Sullivan, R. C.; Carrico, C. M.; Koehler, K. A.;
446 Ziemann, P. J. Role of Molecular Size in Cloud Droplet Activation. *Geophys. Res. Lett.* **2009**, *36*,
447 L22801.
- 448 (20) Jimenez, J. L.; Canagaratna, M. R.; Donahue, N. M.; Prevot, A. S. H.; Zhang, Q.; Kroll, J. H.;
449 DeCarlo, P. F.; Allan, J. D.; Coe, H.; Ng, N. L. et al. Evolution of Organic Aerosols in the
450 Atmosphere. *Science* **2009**, *326*, 1525–9.
- 451 (21) Zhang, Q.; Jimenez, J. L.; Canagaratna, M. R.; Allan, J. D.; Coe, H.; Ulbrich, I.; Alfarra, M. R.;
452 Takami, A.; Middlebrook, A. M.; Sun, Y. L. et al. Ubiquity and Dominance of Oxygenated Species in
453 Organic Aerosols in Anthropogenically-influenced Northern Hemisphere Midlatitudes. *Geophys. Res.*
454 *Lett.* **2007**, *34*, L13801.
- 455 (22) Jacobson, M. C.; Hansson, H.-C.; Noone, K. J.; Charlson, R. J. Organic Atmospheric Aerosols:
456 Review and State of the Science. *Rev. Geophys.* **2000**, *38*, 267.
- 457 (23) Saxena, P.; Hildemann, L. M. Water-Soluble Organics in Atmospheric Particles : A Critical Review
458 of the Literature and Application of Thermodynamics to Identify Candidate Compounds. *J. Atmos.*
459 *Chem.* **1996**, *24*, 57–109.
- 460 (24) Topping, D.; Connolly, P.; McFiggans, G. Cloud Droplet Number Enhanced by Co-condensation of
461 Organic Vapours. *Nat. Geosci.* **2013**, *6*, 443–446.
- 462 (25) You, Y.; Renbaum-Wolff, L.; Carreras-Sospedra, M.; Hanna, S. J.; Hiranuma, N.; Kamal, S.; Smith,
463 M. L.; Zhang, X.; Weber, R. J.; Shilling, J. E. et al. Images Reveal That Atmospheric Particles Can
464 Undergo Liquid-liquid Phase Separations. *Proc. Natl. Acad. Sci. USA* **2012**, *109*, 13188–93.

- 465 (26) Ruehl, C. R.; Chuang, P. Y.; Nenes, A.; Cappa, C. D.; Kolesar, K. R.; Goldstein, A. H. Strong
466 Evidence of Surface Tension Reduction in Microscopic Aqueous Droplets. *Geophys. Res. Lett.* **2012**,
467 39.
- 468 (27) Stokes, R. H.; Robinson, R. A. Interactions in Aqueous Nonelectrolyte Solutions. I. Solute-Solvent
469 Equilibria. *J. Phys. Chem.* **1966**, *70*, 2126–2131.
- 470 (28) Petters, M. D.; Kreidenweis, S. M. A Single Parameter Representation of Hygroscopic Growth and
471 Cloud Condensation Nucleus Activity – Part 3: Including Surfactant Partitioning. *Atmos. Chem. Phys.*
472 **2013**, *13*, 1081–1091.
- 473 (29) Vestin, A.; Rissler, J.; Swietlicki, E.; Frank, G. P.; Andreae, M. O. Cloud-nucleating Properties of the
474 Amazonian Biomass Burning Aerosol: Cloud Condensation Nuclei Measurements and Modeling. *J.*
475 *Geophys. Res.* **2007**, *112*, D14201.
- 476 (30) Wex, H.; Hennig, T.; Salma, I.; Ocskay, R.; Kiselev, A.; Henning, S.; Massling, A.; Wiedensohler,
477 A.; Stratmann, F. Hygroscopic Growth and Measured and Modeled Critical Super-saturations of an
478 Atmospheric HULIS Sample. *Geophys. Res. Lett.* **2007**, *34*, L02818.
- 479 (31) Carrico, C. M.; Petters, M. D.; Kreidenweis, S. M.; Collett, J. L.; Engling, G.; Malm, W. C. Aerosol
480 Hygroscopicity and Cloud Droplet Activation of Extracts of Filters from Biomass Burning
481 Experiments. *J. Geophys. Res.* **2008**, *113*, D08206.
- 482 (32) Duplissy, J.; Gysel, M.; Alfarra, M. R.; Dommen, J.; Metzger, A.; Prevot, A. S. H.; Weingartner, E.;
483 Laaksonen, A.; Raatikainen, T.; Good, N. et al. Cloud Forming Potential of Secondary Organic
484 Aerosol Under Near Atmospheric Conditions. *Geophys. Res. Lett.* **2008**, *35*, 1–5.
- 485 (33) Petters, M. D.; Carrico, C. M.; Kreidenweis, S. M.; Prenni, A. J.; DeMott, P. J.; Collett, J. L.;
486 Moosmüller, H. Cloud Condensation Nucleation Activity of Biomass Burning Aerosol. *J. Geophys.*
487 *Res.* **2009**, *114*, D22205.
- 488 (34) Mochida, M.; Nishita-Hara, C.; Kitamori, Y.; Aggarwal, S. G.; Kawamura, K.; Miura, K.; Takami, A.
489 Size-segregated Measurements of Cloud Condensation Nucleus Activity and Hygroscopic Growth for
490 Aerosols at Cape Hedo, Japan, in Spring 2008. *J. Geophys. Res.* **2010**, *115*, D21207.
- 491 (35) Wex, H.; Fuentes, E.; Tsagkogeorgas, G.; Voigtländer, J.; Clauss, T.; Kiselev, A.; Green, D. H.; Coe,
492 H.; McFiggans, G.; Stratmann, F. The Influence of Algal Exudate on the Hygroscopicity of Sea Spray
493 Particles. *Adv. Meteor.* **2010**, *2010*, 1–11.
- 494 (36) Engelhart, G. J.; Nenes, A.; Pandis, S. N. CCN Activity and Droplet Growth Kinetics of Fresh and
495 Aged Monoterpene Secondary Organic Aerosol. *Atmos. Chem. Phys.* **2008**, *8*, 3937–3949.
- 496 (37) Moore, R. H.; Ingall, E. D.; Sorooshian, A.; Nenes, A. Molar Mass, Surface Tension, and Droplet
497 Growth Kinetics of Marine Organics from Measurements of CCN Activity. *Geophys. Res. Lett.* **2008**,
498 35.
- 499 (38) King, S. M.; Rosenoern, T.; Shilling, J. E.; Chen, Q.; Martin, S. T. Increased Cloud Activation
500 Potential of Secondary Organic Aerosol for Atmospheric Mass Loadings. *Atmos. Chem. Phys.* **2009**,
501 9, 2959–2972.

- 502 (39) Wex, H.; Petters, M. D.; Carrico, C. M.; Hallbauer, E.; Massling, A.; Mcmeeking, G. R.; Poulain, L.;
503 Wu, Z. Towards Closing the Gap Between Hygroscopic Growth and Activation for Secondary
504 Organic Aerosol : Part 1 – Evidence from Measurements. *Atmos. Chem. Phys.* **2009**, *9*, 3987–3997.
- 505 (40) Good, N.; Topping, D. O.; Allan, J. D.; Flynn, M.; Fuentes, E.; Irwin, M.; Williams, P. I.; Coe, H.
506 Consistency Between Parameterisations of Aerosol Hygroscopicity and CCN Activity During the
507 RHaMBLe Discovery Cruise. *Atmos. Chem. Phys.* **2010**, *10*, 3189–3203.
- 508 (41) Irwin, M.; Good, N.; Crosier, J.; Choularton, T. W.; McFiggans, G. Reconciliation of Measurements
509 of Hygroscopic Growth and Critical Supersaturation of Aerosol Particles in Central Germany. *Atmos.*
510 *Chem. Phys.* **2010**, *10*, 11737–11752.
- 511 (42) Padró, L. T.; Tkacik, D.; Lathem, T.; Hennigan, C. J.; Sullivan, A. P.; Weber, R. J.; Huey, L. G.;
512 Nenes, A. Investigation of Cloud Condensation Nuclei Properties and Droplet Growth Kinetics of the
513 Water-soluble Aerosol Fraction in Mexico City. *J. Geophys. Res.* **2010**, *115*, D09204.
- 514 (43) Prenni, A. J.; Petters, M. D.; Kreidenweis, S. M.; DeMott, P. J.; Ziemann, P. J. Cloud Droplet
515 Activation of Secondary Organic Aerosol. *J. Geophys. Res.* **2007**, *112*.
- 516 (44) Petters, M. D.; Wex, H.; Carrico, C. M.; Hallbauer, E.; Massling, A.; Mcmeeking, G. R.; Poulain, L.;
517 Wu, Z. Towards Closing the Gap Between Hygroscopic Growth and Activation for Secondary
518 Organic Aerosol – Part 2 : Theoretical Approaches. *Atmos. Chem. Phys.* **2009**, *9*, 3999–4009.
- 519 (45) Sjogren, S.; Gysel, M.; Weingartner, E.; Baltensperger, U.; Cubison, M. J.; Coe, H.; Zardini, A. A.;
520 Marcolli, C.; Krieger, U. K.; Peter, T. Hygroscopic Growth and Water Uptake Kinetics of Two-phase
521 Aerosol Particles Consisting of Ammonium Sulfate, Adipic and Humic Acid Mixtures. *J. Aerosol Sci.*
522 **2007**, *38*, 157–171.
- 523 (46) Good, N.; Topping, D. O.; Duplissy, J.; Gysel, M.; Meyer, N. K.; Metzger, A.; Turner, S. F.;
524 Baltensperger, U.; Ristovski, Z.; Weingartner, E. et al. Widening the Gap Between Measurement and
525 Modelling of Secondary Organic Aerosol Properties? *Atmos. Chem. Phys.* **2010**, *10*, 2577–2593.
- 526 (47) Petters, M. D.; Kreidenweis, S. M. A Single Parameter Representation of Hygroscopic Growth and
527 Cloud Condensation Nucleus Activity – Part 2 : Including Solubility. *Atmos. Chem. Phys.* **2008**, *8*,
528 5939–5955.
- 529 (48) Duplissy, J.; Gysel, M.; Sjogren, S.; Meyer, N.; Good, N.; Kammermann, L.; Michaud, V.; Weigel,
530 R.; Martins dos Santos, S.; Gruening, C. et al. Intercomparison Study of Six HTDMAs: Results and
531 Recommendations. *Atmos. Meas. Tech.* **2009**, *2*, 363–378.
- 532 (49) Rose, D.; Gunthe, S. S.; Mikhailov, E.; Frank, G. P.; Dusek, U.; Andreae, M. O. Calibration and
533 Measurement Uncertainties of a Continuous-flow Cloud Condensation Nuclei Counter (DMT-
534 CCNC): CCN Activation of Ammonium Sulfate and Sodium Chloride Aerosol Particles in Theory
535 and Experiment. *Atmos. Chem. Phys.* **2008**, *8*, 1153–1179.
- 536 (50) Walker, J. S.; Wills, J. B.; Reid, J. P.; Wang, L.; Topping, D. O.; Butler, J. R.; Zhang, Y.-H. Direct
537 Comparison of the Hygroscopic Properties of Ammonium Sulfate and Sodium Chloride Aerosol at
538 Relative Humidities Approaching Saturation. *J. Phys. Chem. A* **2010**, *114*, 12682–91.

- 539 (51) Fredenslund, A.; Jones, R. L.; Prausnitz, J. M. Group-Contribution Estimation of Activity
540 Coefficients in Nonideal Liquid Mixtures. *AIChE J.* **1975**, *21*, 1086–1099.
- 541 (52) Ruehl, C. R.; Chuang, P. Y.; Nenes, A. Aerosol Hygroscopicity at High (99 to 100%) Relative
542 Humidities. *Atmos. Chem. Phys.* **2010**, *10*, 1329–1344.
- 543 (53) Chang, R. Y.-W.; Slowik, J. G.; Shantz, N. C.; Vlasenko, A.; Liggi, J.; Sjostedt, S. J.; Leitch, W.
544 R.; Abbatt, J. P. D. The Hygroscopicity Parameter (κ) of Ambient Organic Aerosol at a Field Site
545 Subject to Biogenic and Anthropogenic Influences: Relationship to Degree of Aerosol Oxidation.
546 *Atmos. Chem. Phys.* **2010**, *10*, 5047–5064.
- 547 (54) Aiken, A. C.; Decarlo, P. F.; Kroll, J. H.; Worsnop, D. R.; Huffman, J. A.; Docherty, K. S.; Ulbrich,
548 I. M.; Mohr, C.; Kimmel, J. R.; Sueper, D. et al. O/C and OM/OC Ratios of Primary, Secondary, and
549 Ambient Organic Aerosols with High-resolution Time-of-flight Aerosol Mass Spectrometry. *Environ.*
550 *Sci. Technol.* **2008**, *42*, 4478–85.
- 551 (55) Dennis-Smith, B. J.; Miles, R. E. H.; Reid, J. P. Oxidative Aging of Mixed Oleic Acid/sodium
552 Chloride Aerosol Particles. *J. Geophys. Res., [Atmos.]* **2012**, *117*.
- 553 (56) Hanford, K. L.; Mitchem, L.; Reid, J. P.; Clegg, S. L.; Topping, D. O.; McFiggans, G. B.
554 Comparative Thermodynamic Studies of Aqueous Glutaric Acid, Ammonium Sulfate and Sodium
555 Chloride Aerosol at High Humidity. *J. Phys. Chem. A* **2008**, *112*, 9413–22.
- 556 (57) Hargreaves, G.; Kwamena, N.-O. A.; Zhang, Y. H.; Butler, J. R.; Rushworth, S.; Clegg, S. L.; Reid, J.
557 P. Measurements of the Equilibrium Size of Supersaturated Aqueous Sodium Chloride Droplets at
558 Low Relative Humidity Using Aerosol Optical Tweezers and an Electrodynamic Balance. *J. Phys.*
559 *Chem. A* **2010**, *114*, 1806–15.
- 560 (58) Miles, R. E. H.; Walker, J. S.; Burnham, D. R.; Reid, J. P. Retrieval of the Complex Refractive Index
561 of Aerosol Droplets from Optical Tweezers Measurements. *Phys. Chem. Chem. Phys.* **2012**, *14*,
562 3037–3047.
- 563 (59) Preston, T. C.; Reid, J. P. Accurate and Efficient Determination of the Radius, Refractive Index and
564 Dispersion of a Weakly Absorbing Spherical Particle Using Whispering Gallery Modes. *J. Opt. Soc.*
565 *Am. B* **2013**, *In Press*.
- 566 (60) Davies, J. F.; Haddrell, A. E.; Miles, R. E. H.; Bull, C. R.; Reid, J. P. Bulk, Surface, and Gas-phase
567 Limited Water Transport in Aerosol. *J. Phys. Chem. A* **2012**, *116*, 10987–98.
- 568 (61) Davies, J. F.; Haddrell, A. E.; Rickards, A. M. J.; Reid, J. P. Simultaneous Analysis of the
569 Equilibrium Hygroscopicity and Water Transport Kinetics of Liquid Aerosol. *Anal. Chem.* **2013**.
- 570 (62) Glantschnig, W. J.; Chen, S. H. Light Scattering from Water Droplets in the Geometrical Optics
571 Approximation. *Appl. Opt.* **1981**, *20*, 2499–509.
- 572 (63) Davies, J. F.; Haddrell, A. E.; Reid, J. P. Time-Resolved Measurements of the Evaporation of
573 Volatile Components from Single Aerosol Droplets. *Aerosol Sci. Technol.* **2012**, *46*, 666–677.
- 574 (64) Kulmala, M.; Vesala, T.; Wagner, P. E. An Analytical Expression For the Rate of Binary
575 Condensational Particle Growth. *Proc. R. Soc. Lond. A* **1993**, *441*, 589–605.

- 576 (65) Miles, R. E. H.; Reid, J. P.; Riipinen, I. Comparison of Approaches for Measuring the Mass
577 Accommodation Coefficient for the Condensation of Water and Sensitivities to Uncertainties in
578 Thermophysical Properties. *J. Phys. Chem. A* **2012**, *116*, 10810–25.
- 579 (66) Lambe, A. T.; Onasch, T. B.; Massoli, P.; Croasdale, D. R.; Wright, J. P.; Ahern, A. T.; Williams, L.
580 R.; Worsnop, D. R.; Brune, W. H.; Davidovits, P. Laboratory Studies of the Chemical Composition
581 and Cloud Condensation Nuclei (CCN) Activity of Secondary Organic Aerosol (SOA) and Oxidized
582 Primary Organic Aerosol (OPOA). *Atmos. Chem. Phys.* **2011**, *11*, 8913–8928.
- 583 (67) Wong, J. P. S.; Lee, A. K. Y.; Slowik, J. G.; Cziczo, D. J.; Leaitch, W. R.; Macdonald, A.; Abbatt, J.
584 P. D. Oxidation of Ambient Biogenic Secondary Organic Aerosol by Hydroxyl Radicals: Effects on
585 Cloud Condensation Nuclei Activity. *Geophys. Res. Lett.* **2011**, *38*, L22805.
- 586 (68) Cappa, C. D.; Che, D. L.; Kessler, S. H.; Kroll, J. H.; Wilson, K. R. Variations in Organic Aerosol
587 Optical and Hygroscopic Properties Upon Heterogeneous OH Oxidation. *J. Geophys. Res.* **2011**, *116*,
588 1–12.
- 589 (69) Mihara, T.; Mochida, M. Characterization of Solvent-extractable Organics in Urban Aerosols Based
590 on Mass Spectrum Analysis and Hygroscopic Growth Measurement. *Environ. Sci. Technol.* **2011**, *45*,
591 9168–74.
- 592 (70) Hasenkopf, C. A.; Freedman, M. A.; Beaver, M. R.; Toon, O. B.; Tolbert, M. A. Potential Climatic
593 Impact of Organic Haze on Early Earth. *Astrobiology* **2011**, *11*, 135–49.
- 594 (71) Tritscher, T.; Dommen, J.; DeCarlo, P. F.; Gysel, M.; Barmet, P. B.; Praplan, A. P.; Weingartner, E.;
595 Prévôt, A. S. H.; Riipinen, I.; Donahue, N. M. et al. Volatility and Hygroscopicity of Aging
596 Secondary Organic Aerosol in a Smog Chamber. *Atmos. Chem. Phys.* **2011**, *11*, 11477–11496.
- 597 (72) Tritscher, T.; Jurányi, Z.; Martin, M.; Chirico, R.; Gysel, M.; Heringa, M. F.; DeCarlo, P. F.; Sierau,
598 B.; Prévôt, A. S. H.; Weingartner, E. et al. Changes of Hygroscopicity and Morphology During
599 Ageing of Diesel Soot. *Environ. Res. Lett.* **2011**, *6*, 034026.
- 600 (73) Massoli, P.; Lambe, A. T.; Ahern, A. T.; Williams, L. R.; Ehn, M.; Mikkilä, J.; Canagaratna, M. R.;
601 Brune, W. H.; Onasch, T. B.; Jayne, J. T. et al. Relationship Between Aerosol Oxidation Level and
602 Hygroscopic Properties of Laboratory Generated Secondary Organic Aerosol (SOA) Particles.
603 *Geophys. Res. Lett.* **2010**, *37*, 1–5.
- 604 (74) Mikhailov, E.; Vlasenko, S.; Martin, S. T.; Koop, T. Amorphous and Crystalline Aerosol Particles
605 Interacting with Water Vapor: Conceptual Framework and Experimental Evidence for Restructuring,
606 Phase Transitions and Kinetic Limitations. *Atmos. Chem. Phys.* **2009**, *9*, 9491–9522.
- 607 (75) Lang-Yona, N.; Rudich, Y.; Mentel, T. F.; Bohne, A.; Buchholz, A.; Kiendler-Scharr, A.; Kleist, E.;
608 Spindler, C.; Tillmann, R.; Wildt, J. The Chemical and Microphysical Properties of Secondary
609 Organic Aerosols from Holm Oak Emissions. *Atmos. Chem. Phys.* **2010**, *10*, 7253–7265.
- 610 (76) Hersey, S. P.; Craven, J. S.; Schilling, K. A.; Metcalf, A. R.; Sorooshian, A.; Chan, M. N.; Flagan, R.
611 C.; Seinfeld, J. H. The Pasadena Aerosol Characterization Observatory (PACO): Chemical and
612 Physical Analysis of the Western Los Angeles Basin Aerosol. *Atmos. Chem. Phys.* **2011**, *11*, 7417–
613 7443.

- 614 (77) Sorooshian, A.; Murphy, S. M.; Hersey, S.; Gates, H.; Padro, L. T.; Nenes, A.; Brechtel, F. J.;
615 Jonsson, H.; Flagan, R. C.; Seinfeld, J. H. Comprehensive Airborne Characterization of Aerosol from
616 a Major Bovine Source. *Atmos. Chem. Phys.* **2008**, *8*, 5489–5520.
- 617 (78) Poulain, L.; Wu, Z.; Petters, M. D.; Wex, H.; Hallbauer, E.; Wehner, B.; Massling, A.; Kreidenweis,
618 S. M.; Stratmann, F. Towards Closing the Gap Between Hygroscopic Growth and CCN Activation
619 for Secondary Organic Aerosols – Part 3: Influence of the Chemical Composition on the Hygroscopic
620 Properties and Volatile Fractions of Aerosols. *Atmos. Chem. Phys.* **2010**, *10*, 3775–3785.
- 621 (79) Moore, R. H.; Raatikainen, T.; Langridge, J. M.; Bahreini, R.; Brock, C. A.; Holloway, J. S.; Lack, D.
622 A.; Middlebrook, A. M.; Perring, A. E.; Schwarz, J. P. et al. CCN Spectra, Hygroscopicity, and
623 Droplet Activation Kinetics of Secondary Organic Aerosol Resulting from the 2010 Deepwater
624 Horizon Oil Spill. *Environ. Sci. Technol.* **2012**, *46*, 3093–100.
- 625 (80) Tang, X.; Zheng, Z.; Jung, H. S.; Asa-Awuku, A. The Effects of Mainstream and Sidestream
626 Environmental Tobacco Smoke Composition for Enhanced Condensational Droplet Growth by Water
627 Vapor. *Aerosol Sci. Technol.* **2012**, *46*, 760–766.
- 628 (81) Engelhart, G. J.; Moore, R. H.; Nenes, A.; Pandis, S. N. Cloud Condensation Nuclei Activity of
629 Isoprene Secondary Organic Aerosol. *J. Geophys. Res.* **2011**, *116*, 1–11.
- 630 (82) Frosch, M.; Bilde, M.; DeCarlo, P. F.; Jurányi, Z.; Tritscher, T.; Dommen, J.; Donahue, N. M.; Gysel,
631 M.; Weingartner, E.; Baltensperger, U. Relating Cloud Condensation Nuclei Activity and Oxidation
632 Level of α -pinene Secondary Organic Aerosols. *J. Geophys. Res.* **2011**, *116*, D22212.
- 633 (83) Kuwata, M.; Chen, Q.; Martin, S. T. Cloud Condensation Nuclei (CCN) Activity and Oxygen-to-
634 carbon Elemental Ratios Following Thermodenuder Treatment of Organic Particles Grown by α -
635 pinene Ozonolysis. *Phys. Chem. Chem. Phys.* **2011**, *13*, 14571–83.
- 636 (84) Lambe, A. T.; Ahern, A. T.; Williams, L. R.; Slowik, J. G.; Wong, J. P. S.; Abbatt, J. P. D.; Brune,
637 W. H.; Ng, N. L.; Wright, J. P.; Croasdale, D. R. et al. Characterization of Aerosol Photooxidation
638 Flow Reactors: Heterogeneous Oxidation, Secondary Organic Aerosol Formation and Cloud
639 Condensation Nuclei Activity Measurements. *Atmos. Meas. Tech.* **2011**, *4*, 445–461.
- 640 (85) Moore, R. H.; Bahreini, R.; Brock, C. A.; Froyd, K. D.; Cozic, J.; Holloway, J. S.; Middlebrook, A.
641 M.; Murphy, D. M.; Nenes, A. Hygroscopicity and Composition of Alaskan Arctic CCN During April
642 2008. *Atmos. Chem. Phys.* **2011**, *11*, 11807–11825.
- 643 (86) Frosch, M.; Zardini, A. A.; Platt, S. M.; Müller, L.; Reinnig, M.-C.; Hoffmann, T.; Bilde, M.
644 Thermodynamic Properties and Cloud Droplet Activation of a Series of Oxo-acids. *Atmos. Chem.*
645 *Phys.* **2010**, *10*, 5873–5890.
- 646 (87) George, I. J.; Abbatt, J. P. D. Chemical Evolution of Secondary Organic Aerosol from OH-initiated
647 Heterogeneous Oxidation. *Atmos. Chem. Phys.* **2010**, *10*, 5551–5563.
- 648 (88) King, S. M.; Rosenoern, T.; Shilling, J. E.; Chen, Q.; Wang, Z.; Biskos, G.; McKinney, K. A.; Pöschl,
649 U.; Martin, S. T. Cloud Droplet Activation of Mixed Organic-sulfate Particles Produced by the
650 Photooxidation of Isoprene. *Atmos. Chem. Phys.* **2010**, *10*, 3953–3964.

- 651 (89) Roberts, G. C.; Day, D. A.; Russell, L. M.; Dunlea, E. J.; Jimenez, J. L.; Tomlinson, J. M.; Collins, D.
652 R.; Shinozuka, Y.; Clarke, A. D. Characterization of Particle Cloud Droplet Activity and
653 Composition in the Free Troposphere and the Boundary Layer During INTEX-B. *Atmos. Chem. Phys.*
654 **2010**, *10*, 6627–6644.
- 655 (90) Haynes, W. M. Section 5: Thermochemistry, Electrochemistry, and Kinetics. In *CRC Handbook of*
656 *Chemistry and Physics*; pp. 154–189.
- 657 (91) Gaivoronskii, A. N.; Granzhan, V. A. Solubility of Adipic Acid in Organic Solvents and Water. *Russ.*
658 *J. Appl. Chem.* **2005**, *78*, 404–408.
- 659 (92) Attané, E. C.; Doumani, T. F. Solubilities of Aliphatic Dicarboxylic Acids in Water. *Ind. Eng. Chem.*
660 **1949**, 2015–2017.
- 661 (93) Higashiyama, T. Novel Functions and Applications of Trehalose. *Pure Appl. Chem.* **2002**, *74*, 1263–
662 1269.
- 663

664 **TABLES**

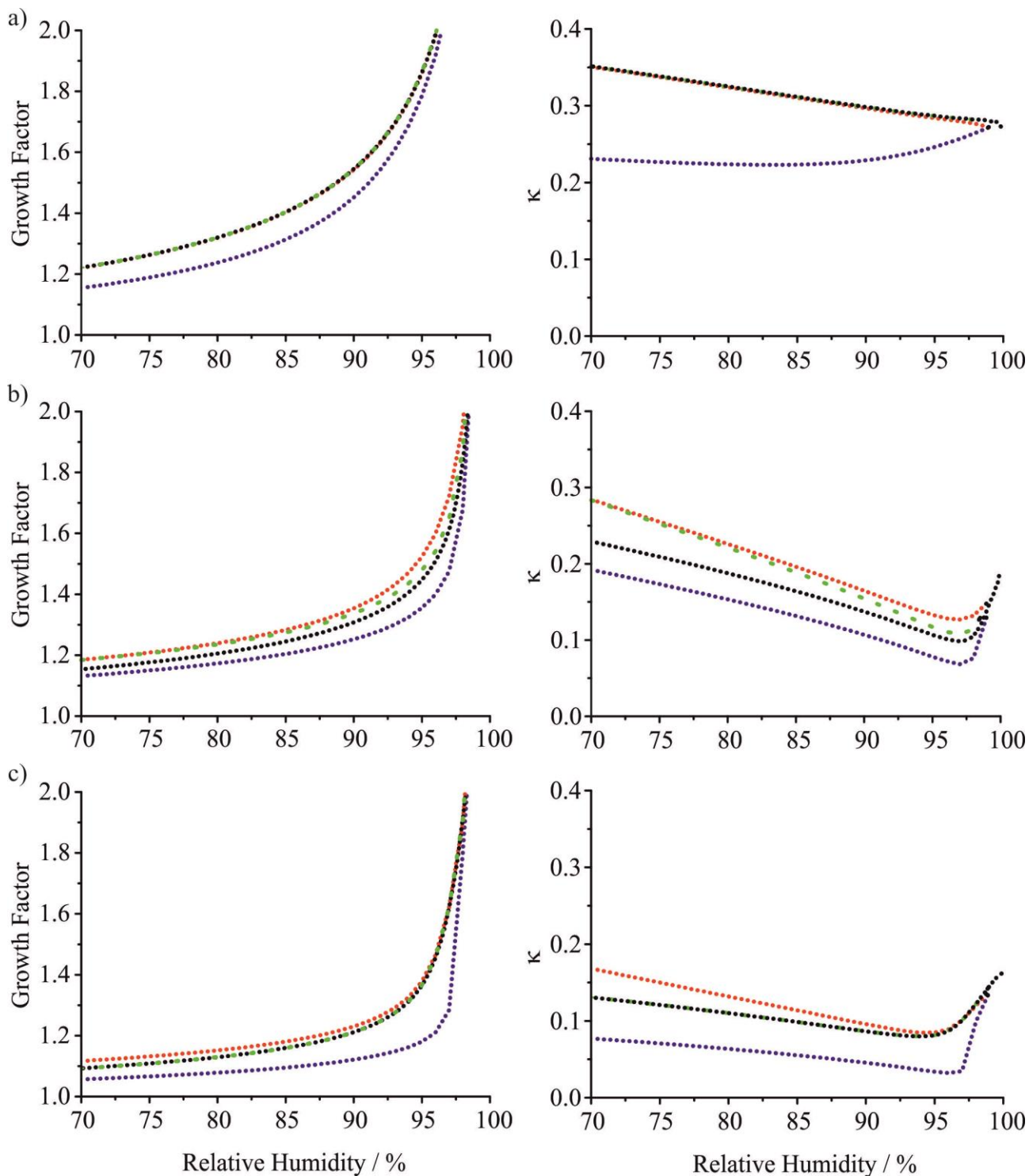
665 Table 1: A list of organic compounds for which hygroscopic growth was determined. Solubility data are
 666 taken from (a) the CRC Handbook of Chemistry and Physics,⁹⁰ (b) Gaivoronskii and Granzhan,⁹¹ (c) Attané
 667 and Doumani,⁹² and (d) Higashiyama,⁹³ with the measurement temperature in superscript. All compounds
 668 were sourced from Sigma-Aldrich, with the exception of glutaric acid (Acros Organics), maleic acid (Acros
 669 Organics), and citric acid (Fisher Scientific). The experimental technique used to determine κ is given and
 670 those values are presented in the final column along with the corresponding a_w .

Compound	O/C	Solubility by mass	Technique	κ ($a_w \pm 0.02$)
Oleic acid (C ₁₈ H ₃₄ O ₂ , >90 %)	0.11	-	AOT	0.003 ± 0.001 (0.60 - 0.75)
Adipic acid (C ₆ H ₁₀ O ₄ , ≥ 99.5 %)	0.67	1.8 %, b ^{20°C}	EDB	0.102 ± 0.009 (> 0.90)
Glutaric acid (C ₅ H ₈ O ₄ , 99 %)	0.80	51 %, c ^{18°C}	EDB	0.168 ± 0.030 (> 0.90)
D-(+)-Raffinose (C ₁₈ H ₃₂ O ₁₆ , ≥ 98.0 %)	0.89	12.5 %, a ^{20°C}	EDB	0.063 ± 0.012 (> (0.90))
Sucrose (C ₁₂ H ₂₂ O ₁₁ , ≥ 99.5 %)	0.92	67.1 %, a ^{20°C}	EDB	0.115 ± 0.005 (> 0.90)
D-(+)-Trehalose (C ₁₂ H ₂₂ O ₁₁ , ≥ 99 %)	0.92	68.9 %, d ^{20°C}	EDB	0.116 ± 0.014 (> 0.90)
L-Ascorbic Acid (C ₆ H ₈ O ₆ , ≥ 99.0 %)	1	25.2 %, a ^{25°C}	AOT	0.192 ± 0.064 (0.80)
D-(+)-Galactose (C ₆ H ₁₂ O ₆ , ≥ 99 %)	1	40.6 %, a ^{20°C}	AOT EDB	0.212 ± 0.045 (0.80) 0.192 ± 0.013 (> 0.90)
D-(+)-Glucose (C ₆ H ₁₂ O ₆ , ≥ 99.5 %)	1	45.0 %, a ^{15°C}	EDB	0.254 ± 0.015 (> 0.90)
Maleic acid (C ₄ H ₄ O ₄ , 99 %)	1	44.1 %, a ^{25°C}	EDB	0.367 ± 0.021 (> 0.90)
D-Sorbitol (C ₆ H ₁₄ O ₆ , ≥ 98 %)	1	41 %, a ^{20°C}	AOT EDB	0.184 ± 0.011 (0.77) 0.154 ± 0.003 (> 0.90)
Succinic acid (C ₄ H ₆ O ₄ , ≥ 99.0 %)	1	7.7 %, a ^{25°C}	EDB	0.216 ± 0.020 (> 0.90)
<i>trans</i> -Aconitic acid (C ₆ H ₆ O ₆ , 98 %)	1	20.9 %, a ^{25°C}	EDB	0.172 ± 0.010 (> 0.90)
D-(+)-Xylose (C ₅ H ₁₀ O ₅ , ≥ 99 %)	1	30 %, a ^{25°C}	AOT	0.179 ± 0.015 (0.78)
Citric acid (C ₆ H ₈ O ₇ , > 99.5 %)	1.17	59 %, a ^{20°C}	AOT	0.233 ± 0.035 (0.66)
Malonic acid (C ₃ H ₄ O ₄ , 99 %)	1.33	42.4 %, a ^{20°C}	EDB	0.292 ± 0.011 (> 0.90)
L-(+)-Tartaric acid (C ₄ H ₆ O ₆ , ≥ 99.5 %)	1.50	58 %, a ^{20°C}	EDB	0.220 ± 0.007 (> 0.90)
Oxalic acid (C ₂ H ₂ O ₄ , ≥ 99.0 %)	2	8.7 %, a ^{20°C}	EDB	0.504 ± 0.044 (> 0.90)

671

672 **FIGURES**

673 Figure 1: (a) Predictions of the change in growth factor with RH and the retrieved value of κ if measure-
 674 ments were made at different RHs for (a) malonic acid, (b) levoglucosan, and (c) adipic acid from UNIFAC
 675 (E-AIM) (blue), UNIFAC with Peng parameters (E-AIM) (green), ADDEM (red) and AIOMFAC (black).
 676

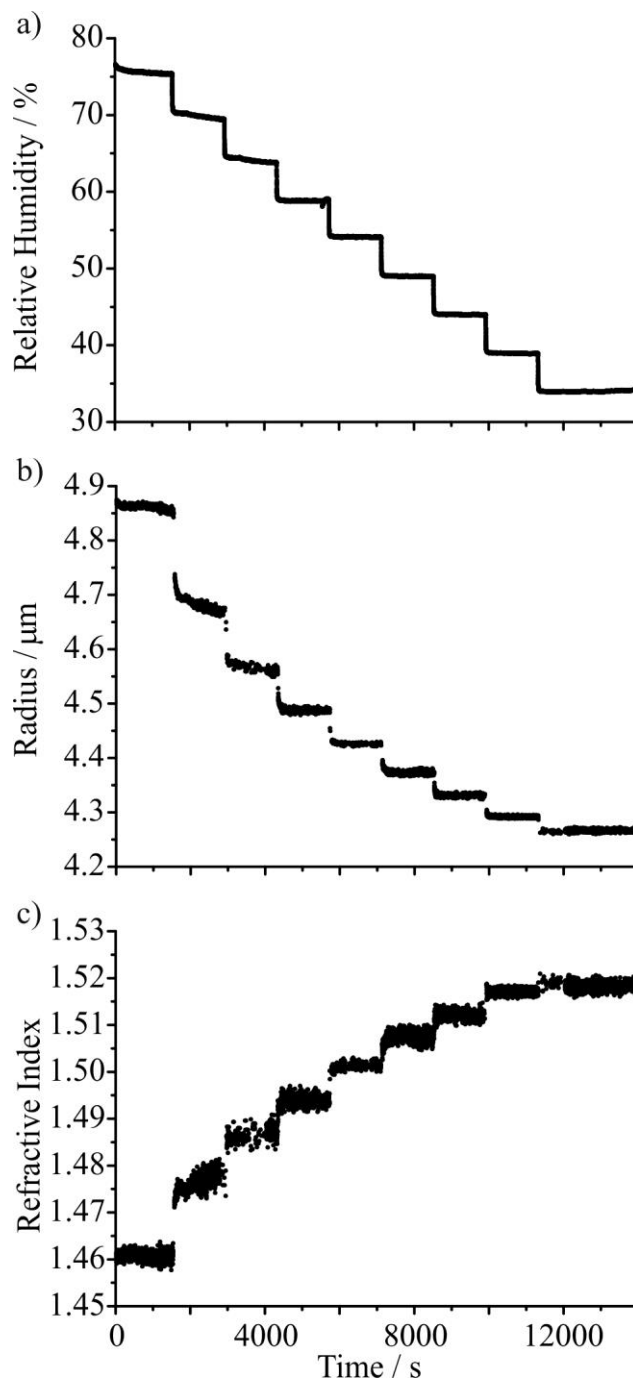


677

678

679 Figure 2: Correlated change in (a) RH, (b) particle radius, and (c) particle RI with time for an aqueous
680 sucrose droplet with dry radius 4145 ± 11 nm held in AOT.

681

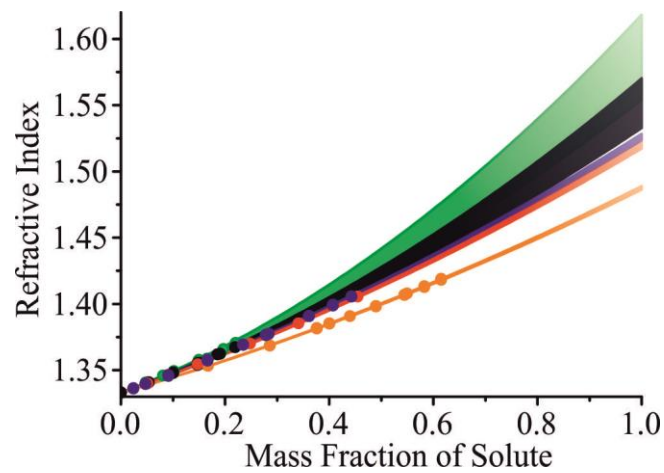


682

683

684 Figure 3: Refractive index values measured using a refractometer plotted against mfs, with
685 quadratic fits applied to the experimental data. Extrapolation to mfs of one yields refractive index
686 values for pure galactose (black), ascorbic acid (green), sorbitol (purple), xylose (red), and citric
687 acid (orange) of 1.5515 ± 0.0187 , 1.5863 ± 0.0320 , 1.5260 ± 0.0024 , 1.5197 ± 0.0024 , and 1.4876
688 ± 0.0013 respectively. The shaded regions represent the standard error in the quadratic fits.
689 Knowledge of the pure component refractive index is vital for determination of the aerosol droplet
690 dry size, and in turn the *GF*.

691

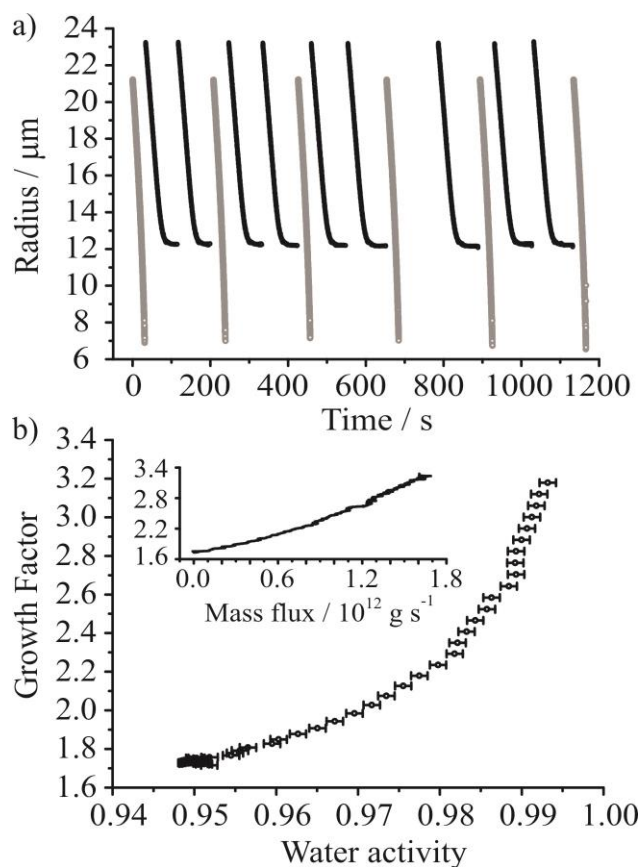


692

693

694 Figure 4: (a) An example of the comparative kinetic measurement showing consecutive evaporation of pure
695 water (grey) and tartaric acid (black) solution droplets into an RH of ~ 0.95 . (b) The growth curve derived
696 from the mass flux data averaged over all tartaric acid droplets and resolved at each size point, with an
697 average taken every 200 points (equivalent to 2 s of mass flux). Uncertainty in GF lies within the bounds of
698 the data points. Inset shows the growth factor as a function of measured mass flux, used to calculate the
699 droplet water activity.

700

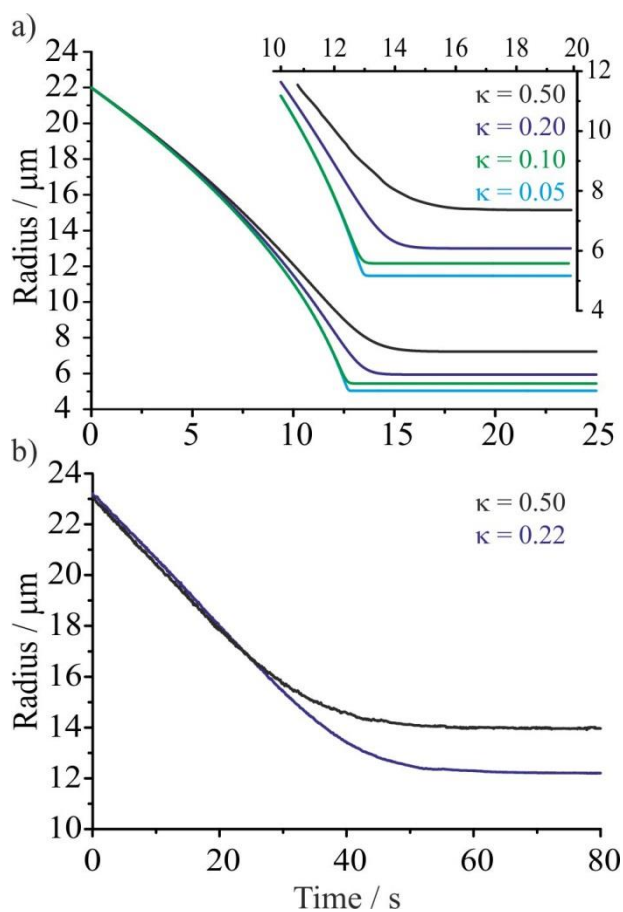


701

702

703 Figure 5: (a) Simulated evaporation profiles for droplets containing a fixed amount of a dissolved species
704 with varying values of κ , illustrating the sensitivity of the EDB evaporation method for measuring
705 hygroscopic growth. The inset shows the long time equilibrium behaviour. We present simulated data in
706 order to show the effect of changing κ while keeping all other variables the same, for instance how the
707 density changes with radius. (b) As an example of the experimental data, measurement data sets of the
708 evaporation kinetics from aqueous droplets of oxalic acid at 93.8 % RH (blue) and tartaric acid at 94.8 % RH
709 (black). Both compounds had an initial concentration of 50.2 g L⁻¹.

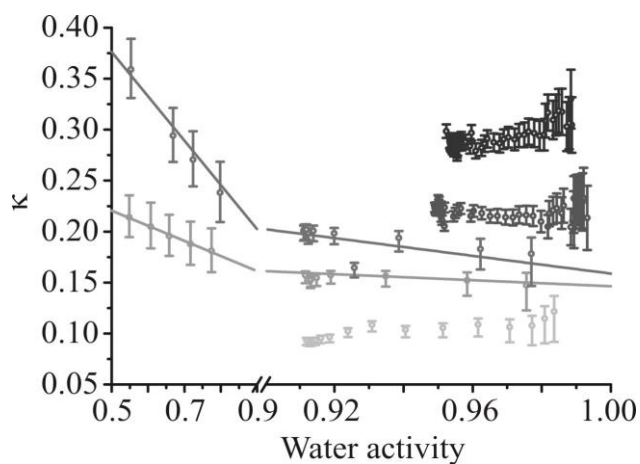
710



711

712

713 Figure 6: A comparison between experimental data obtained from AOT measurements (at lower water
714 activity) and EDB measurements (at higher water activity) for five representative compounds: malonic acid,
715 tartaric acid, galactose, sorbitol and adipic acid (dark to light grey points, top to bottom). The lines associated
716 with galactose and sorbitol represent linear fits using data from both techniques. The break in the water
717 activity axis and the change in scale should be noted.
718

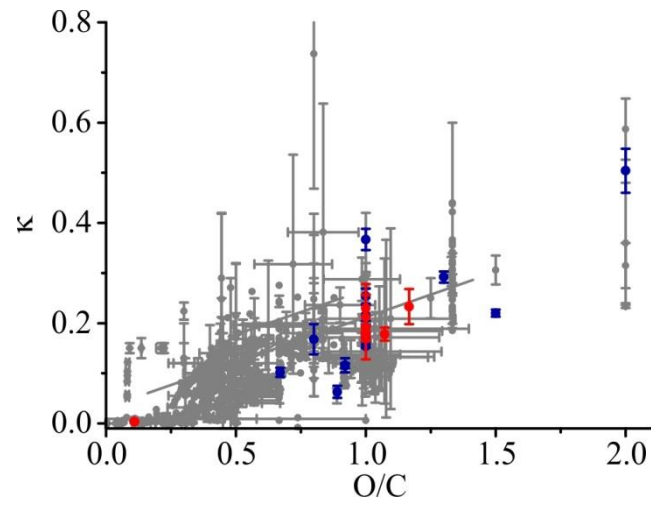


719

720

721 Figure 7: Experimentally determined κ values from AOT (red) and EDB (blue) measurements as a function
722 of O/C and data from the literature survey described in the text (grey).

723

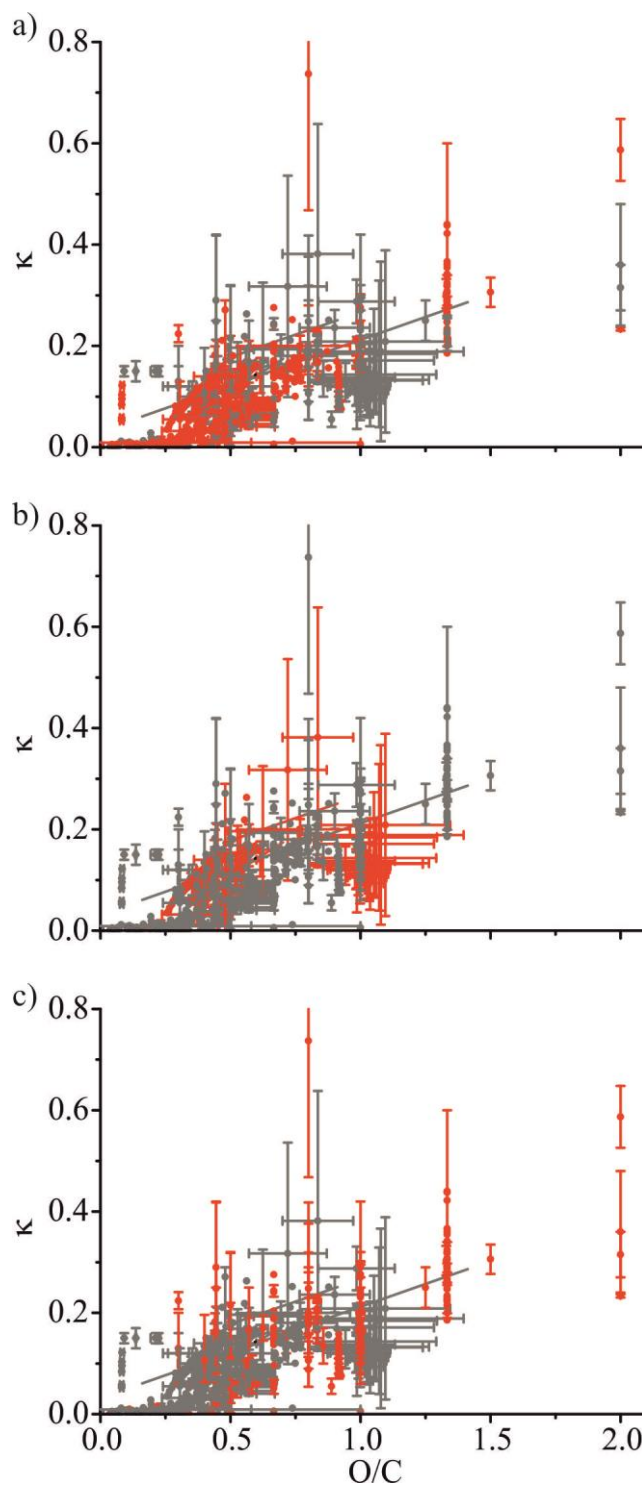


724

725

726 Figure 8: Review of literature data showing the relationship between O/C and κ , with the three
727 panels highlighting data recorded (a) at subsaturated RH (red) and supersaturated RH (grey), (b) in
728 field studies (red) and in laboratory studies (grey) and (c) where the O/C of the aerosol was well-
729 defined (red), and where O/C was inferred from AMS measurements (grey).

730

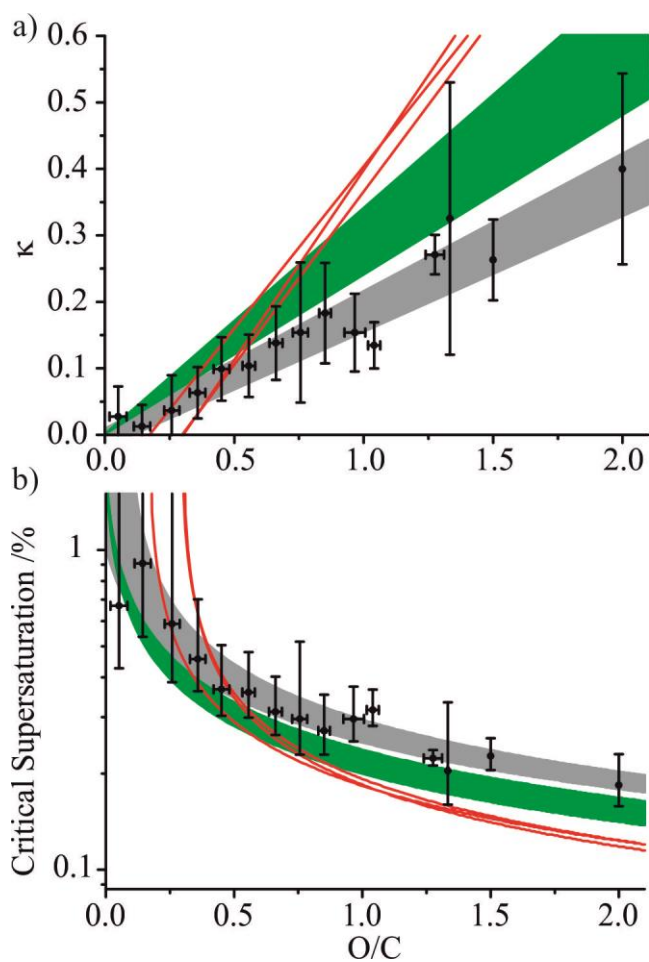


731

732

733 Figure 9: All new experimental and literature data binned by O/C in intervals of 0.1 in terms of (a) κ and (b)
734 predicted critical supersaturation (for a 100 nm diameter aerosol particle). The error bars represent the
735 standard deviation of the average reported κ value, and do not include any experimentally associated error
736 with each of the measurements reported in the literature. A linear fit to this binned data for κ and O/C has
737 been included (grey shaded area), along with previously proposed linear relationships by Chang et al.⁵³
738 (green shaded area) and Duplissy et al.⁷ (red lines).

739

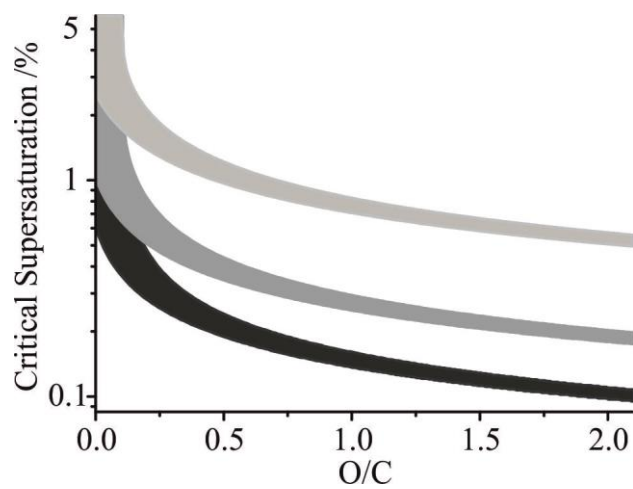


740

741

742 Figure 10: Variation in predicted critical supersaturations with O/C from the linear fit (and uncertainties) to κ
743 for the experimental and literature data. The shaded areas represent aerosol droplets of different dry
744 diameter: 50 nm, 100 nm, and 150 nm, from top to bottom.

745



746